Fundamental role of inferior olive connexin 36 in muscle coherence during tremor

Dimitris G. Placantonakis*†, Anatoly A. Bukovsky‡§, Xiao-Hui Zeng§, Hans-Peter Kiem‡, and John P. Welsh§¶

*Department of Physiology and Neuroscience, New York University School of Medicine, New York, NY 10016; ‡Clinical Research Division, Fred Hutchinson Cancer Research Center, Seattle, WA 98109; and §Neurological Sciences Institute, Oregon Health and Science University, Beaverton, OR 97006

Edited by Rodolfo R. Llinás, New York University Medical Center, New York, NY, and approved March 16, 2004 (received for review January 14, 2004)

Inferior olive (IO) neurons are electrically coupled by cytosolic pores formed by the neuron-specific connexin 36 (Cx36). Electrical coupling in the IO figures prominently in current views about brain control of movement. However, a role for Cx36 in movement has been questioned and not definitively demonstrated. Previous reports have shown that embryonic deletion of the Cx36 gene resulted in almost complete loss of cytosolic and electrical coupling in the IO without an obvious deficit in movement, possibly due to developmental compensations in ionic conductances that can confound the approach of embryonic gene deletion. We used a replication-incompetent lentiviral vector to stably express a dominant-negative Cx36 mutant in the IO of adult rats. We show that interneuronal cytosolic coupling is severely reduced by the mutant Cx36, without effect on neuron morphology or electrical properties. Multisite electromyography revealed that blocking Cx36 in the IO impaired the coherence of muscle firing during harmaline tremor without affecting its rhythm. The data demonstrate that gap junction coupling within the IO mediated by Cx36 adds 10–20 ms of precision to the fine temporal coordination of muscle firing during movement.

Electrical synapses permit neuronal ensembles to fire synchronously with millisecond precision. Connexin 36 (Cx36) is the neuron-specific protein (1) that forms electrical synapses mediated by gap junction pores that link the cytosol of neighboring neurons (2, 3). Although outnumbered by chemical synapses, electrical synapses are distributed widely throughout the brain. Nevertheless, it has not been possible to establish a behavioral function for Cx36 primarily due to the lack of agents that specifically block connexins (4).

In adult brain, Cx36 and electrical synapses are most prevalent in the inferior olive (IO), where dendritic gap junctions underlie electrotonic coupling (5–7). The IO is a precerebellar nucleus that emits rhythmic activity patterns punctuated by a high degree of synchrony, as measured by multiple intracranial microelectrodes (8–10). The spatial pattern of IO synchrony is modulated during skilled movement (9), suggesting that electrical synapses are important for motor coordination. However, embryonic deletion of Cx36 did not detectably impair gross motricity (11) or the tremor produced by harmaline (11, 12), a movement that is generated by rhythmic output from the IO (13, 14). A recent analysis showed that compensatory alterations in ionic conductances might account for the single-cell rhythmicity of electrically uncoupled IO neurons (15) and potentially explain why harmaline tremor persisted in the absence of electrical synapses (11, 12). Thus, the role of Cx36 in the IO for movement remains a compelling question.

To circumvent the morphological and electrophysiological compensations that can confound embryonic gene deletion, we used gene transfer into the adult brain with a replication-incompetent and self-inactivating lentiviral vector (LV; refs. 16–18) to deliver a dominant negative mutant Cx36 into the IO. The mutation of Cx36 consisted of a single amino acid substitution of serine for cysteine, in the putative second extracellular loop of the protein (19). Our previous work in cell cultures showed that this mutation of Cx36 prevents wild-type Cx36 from forming intercellular channels at the membrane, preventing cytosolic coupling (19).

We studied the effect of the dominant-negative Cx36 on cytosolic coupling in the IO and determined the specificity of the LV blocker by carefully examining the electrical properties and the fine morphology of IO neurons. After confirming specificity, we examined the effect of blocking Cx36 on harmaline tremor, a behavior controlled by the IO. We find that Cx36 in the IO promotes the coherence of firing among widely separated muscles during movement.

Materials and Methods

Design and Generation of Recombinant LV. The third generation HIV-1-based LV system (16, 17) was obtained from Cell Genesys (Foster City, CA). The transfer-vector plasmid was modified to contain the central polypurine tract-central termination sequence to increase transduction efficiency (20). LV preparations were generated in 293T cells by calcium phosphate transfection (17). Centrifuged LV was resuspended in PBS supplemented with 1% BSA.

To locate LV-transduced neurons, it was necessary to codeliver a marker gene. In consideration of many reports describing the inefficiency of using an internal ribosome entry site to express two genes from a single promoter, we designed a dual internal-promoter transfer-vector construct. In our construct (termed mutCx36-GFP-LV), two promoter/gene expression elements were cloned sequentially such that the human phosphoglycerate kinase (PGK) promoter drove expression of the mutant Cx36 gene and the murine stem cell virus (MSCV) promoter drove expression of the GFP gene (Fig. 1*a*). We anticipated that transduced cells would express both genes because they were linked in a single transgene with common polyadenylation site in the vector LTR and that their expression would be a function of the corresponding promoter's transcriptional activity. Transduction of COS-7 cells, which lack native Cx36, confirmed that both mutant Cx36 and GFP were efficiently expressed after transduction with mutCx36-GFP-LV (Fig. 1*b*). To control for effects of LV and GFP, we used a similar construct (termed GFP-LV) containing only the GFP gene driven by the PGK promoter. Estimated titers were 4.4×10^8 transducing units/ml (TU/ml) for GFP-LV and 4.5×10^8 TU/ml for mutCx36-GFP-LV in HT1080 cells.

Implantation of LV. Sprague–Dawley rats (6 weeks old, $n = 52$) were anesthetized (100 mg/kg ketamine, 8 mg/kg xylazine, and 0.4 mg/kg atropine), and, for each, the neck was carefully dissected to expose the skull base, which was drilled to expose the ventral brainstem. LV suspension (1–2 μl) was placed into the

This paper was submitted directly (Track II) to the PNAS office.

Abbreviations: IO, inferior olive; Cx36, connexin 36; LV, lentiviral vector; EMG, electromyography; KS, Kolmogorov–Smirnov two-sample test.

†Present address: Department of Neurological Surgery, Weill Cornell Medical Center, New York, NY 10021.

¶To whom correspondence should be addressed. E-mail: welshj@ohsu.edu.

www.pnas.org/cgi/doi/10.1073/pnas.0400322101

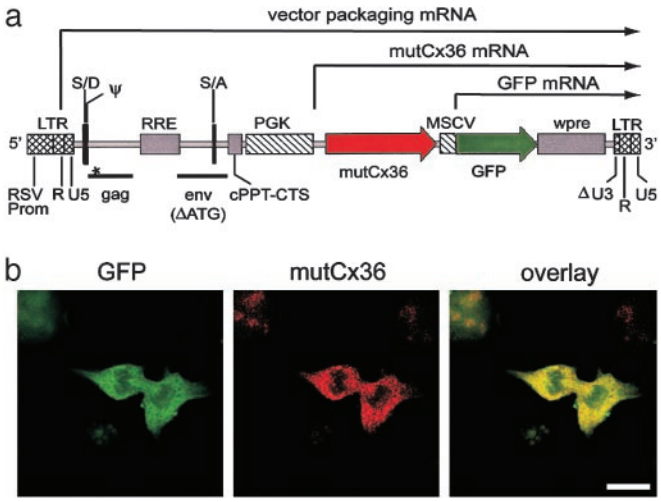

Fig. 1. LV expression of mutant Cx36. (*a*) mutCx36-GFP-LV genome. LTR, long terminal repeat; RSV prom, Rous sarcoma virus promoter; S/D and S/A, splice donor, acceptor; RRE, Rev response element; cPPT-CTS, central polypurine tract-central termination sequence; wpre, woodchuck hepatitis virus post-transcriptional regulatory element; U3, R, and U5, segments of LV LTR; gag and env, LV sequences; Δ, deletion; ATG, initiator codon; *, premature STOP codon in gag sequence; PGK, phosphoglycerate kinase; MSCV, murine stem cell virus. (*b*) Transduction of COS-7 cells by mutCx36-GFP-LV. Mutant Cx36 is visualized with an antibody to wild-type Cx36. (Scale bar = 25 μm.)

medulla by a glass micropipette every 0.2–0.4 mm from 0.0–1.3 mm rostral to the occipital foramen, 0.4–1.0 mm lateral to the basilar artery at 0.4–1.0 mm depth. Injections were bilateral for *in vitro* analysis ($n = 41$) and unilateral into the left IO for *in vivo* analysis ($n = 11$). Measurements were taken 1–4 weeks later.

Immunofluorescence and Confocal Microscopy. Rats were perfused with 4% paraformaldehyde, and the brains were postfixed with 30% sucrose before sectioning (30 μm). Tissue was permeabilized and blocked with solution containing 1% BSA, 10% goat serum, and 0.4% Triton X-100 in Dulbecco's PBS (DPBS). Subsequent antibody incubations were performed in 5% blocking solution in DPBS. Anti-Cx36 (2 μg/ml; Zymed) and anti-calbindin (1:200; Sigma) antibodies were detected with secondary antibodies conjugated to Alexa Fluor 568 or 647 (5 μg/ml; Molecular Probes). Tissue was imaged with a laser scanning confocal microscope (Zeiss LSM-510 META). The GFP emission between 477–541 nm after mutCx36-GFP-LV was 277% higher than background, as determined by fluorescence spectroscopy and 2-photon excitation of GFP at 800 nm (Chameleon, Coherent, Santa Clara, CA). Rendered reconstruction of serial optical sections was performed by Zeiss VISART software. Optical sections of filled IO neurons were used to measure the soma diameter at its long axis and the thickness of the proximal dendrites 5 μm from the soma.

Intracellular Electrophysiology and Cytosolic Coupling. Analyses of cytosolic coupling and morphology were carried out in IO neurons electrophysiologically identified by intracellular recording from brainstem slices maintained alive *in vitro*. Brainstem slice preparation was performed as described (21, 22), except that 300-μm-thick slices were cut in Ringer's solution containing no NaCl, 252 mM sucrose, 0.5 mM $CaCl_2$, and 3.5 mM $MgSO_4$. Identification of an IO neuron required an after depolarizing potential and after hyperpolarization after each spike, and a low-threshold spike when released from hyperpolarization (22, 23). Recordings were made with sharp electrodes and an Axoclamp2B amplifier (Axon Instruments, Foster City, CA) in current clamp mode. Neurobiotin (4% wt/vol in 2 M potassium acetate, Vector Laboratories) fills were made through the electrode by using +4.0-nA current pulses at 0.5 Hz (50% duty cycle) for 20 min. After a 2-h incubation (35°C), slices were fixed in 4% paraformaldehyde overnight, incubated in blocking solution (2 h) and then in 10% blocking solution with 1 μg/ml streptavidin-Alexa Fluor 568 (2–3 days). Injected neurons were identified by their more intense staining (24). Emission spectra of single neurons were made by measuring the fluorescence intensity from 370–720 nm (10-nm resolution).

Electromyography (EMG). In 11 rats, 1–2 weeks after implantation of LV into or near the left IO, bipolar EMG electrodes (51-μm diameter) were inserted into the clavotrapezius, triceps brachii, and latissimus dorsi muscles, bilaterally, under anesthesia, for a total of six EMG sites per rat. Leads were externalized at the scalp, soldered to a connector, and fastened to the skull. After 2–3 days of recovery, EMG recordings (20–30 min) were obtained from the six sites beginning at least 15 min after an injection of harmaline HCl (i.p. 10 mg/kg, Sigma) by using a multichannel recorder (16-bit, 24 kHz per channel; Cygnus, Delaware Water Gap, PA). The potentials were amplified with six differential amplifiers (Biomedical Engineering, Thornwood, NY), by using a screw on the occipital bone as a common reference. Signals were rectified above the baseline and filtered (<100 Hz) before events were detected when the signal exceeded 20 SD of baseline (DATAPAC2K2, Run Technologies, Mission Viejo, CA). Tremor was quantified with auto- and cross-correlation (Nex Technologies, Littleton, MA) in 1- or 5-ms bins. Calculations of tremor frequency and coherence were made for each muscle. Tremor frequency was derived from the auto-correlation histograms by averaging the interpeak intervals of the three successive peaks after time 0 and calculating an instantaneous frequency (e.g., Fig. 5*b*). Coherence was calculated as the inverse of the mean width of the center peak of the cross-correlograms at half-amplitude for all possible ipsilateral combinations (e.g., Fig. 5*d*).

Statistics. Differences between group averages of tremor frequency and coherence were evaluated with ANOVA (25). Kolmogorov–Smirnov two-sample test (KS) was used to evaluate laterality differences between the mean cross-correlation functions from −60 to 60 ms and mean auto-correlation functions from 30 to 300 ms. A *t* test was used to evaluate spike parameters. Significance was set at $P < 0.05$. Data are reported as the mean ± 1 SEM.

Results

Efficient LV Transduction of IO Neurons. Each 1- to 2-μl injection of LV produced an ≈600-μm-diameter transduction zone of GFP-expressing neurons and glia (Fig. 2*a*). That IO neurons were transduced was verified by the colocalization of GFP with the neuron-specific proteins calbindin after mutCx36-GFP-LV (Fig. 2*b*) or Cx36 after GFP-LV (Fig. 2*c*). In zones of mutCx36-GFP-LV, 86 ± 4% of IO neurons were transduced ($n = 20$ fields and 4 rats) whereas IO neurons represented 60 ± 4% of all transduced cells ($n = 18$ fields and 4 rats). In zones of GFP-LV, 76 ± 3% of neurons were transduced ($n = 20$ fields and 4 rats) and neurons comprised 60 ± 6% of transduced cells ($n = 14$ fields and 4 rats). There was no statistical difference in the efficiency of the two LVs.

Mutant Cx36 LV Blocks Cytosolic Coupling. In control brains, injection of Neurobiotin into single electrophysiologically identified (Fig. 3*a*) IO neurons resulted in spread of the dye to 7.8 ± 2.1 neurons ($n = 14$ slices; Fig. 3*b*), replicating previous results (24). To control for the possibility that the spread occurred by means of extracellular leakage, we repeated the experiment after 10–13

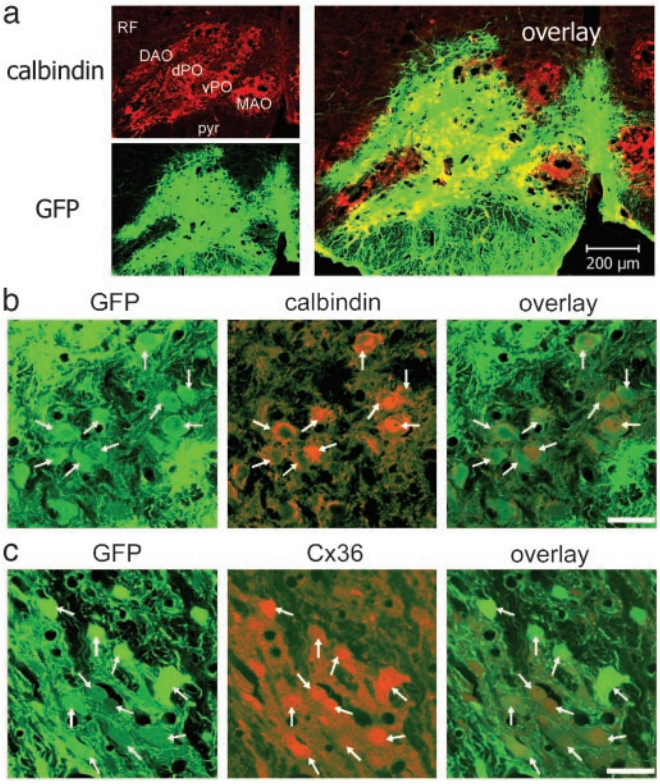

Fig. 2. Transduction of the IO by LVs. (*a*) A zone of LV transduction in the IO. dPO, dorsal lamella principal olive; vPO, ventral lamella principal olive; DAO, dorsal accessory olive; MAO, medial accessory olive; pyr, pyramid; RF, reticular formation. (*b* and *c*) IO neurons (arrows) transduced by mutCx36-GFP-LV (*b*) and GFP-LV (*c*). Transduction of IO neurons is confirmed by the colocalization of GFP with calbindin (red) in *a* and *b*, and with Cx36 (red) in *c*. (Scale bars = 200 μm in *a* and 25 μm in *b* and *c*.)

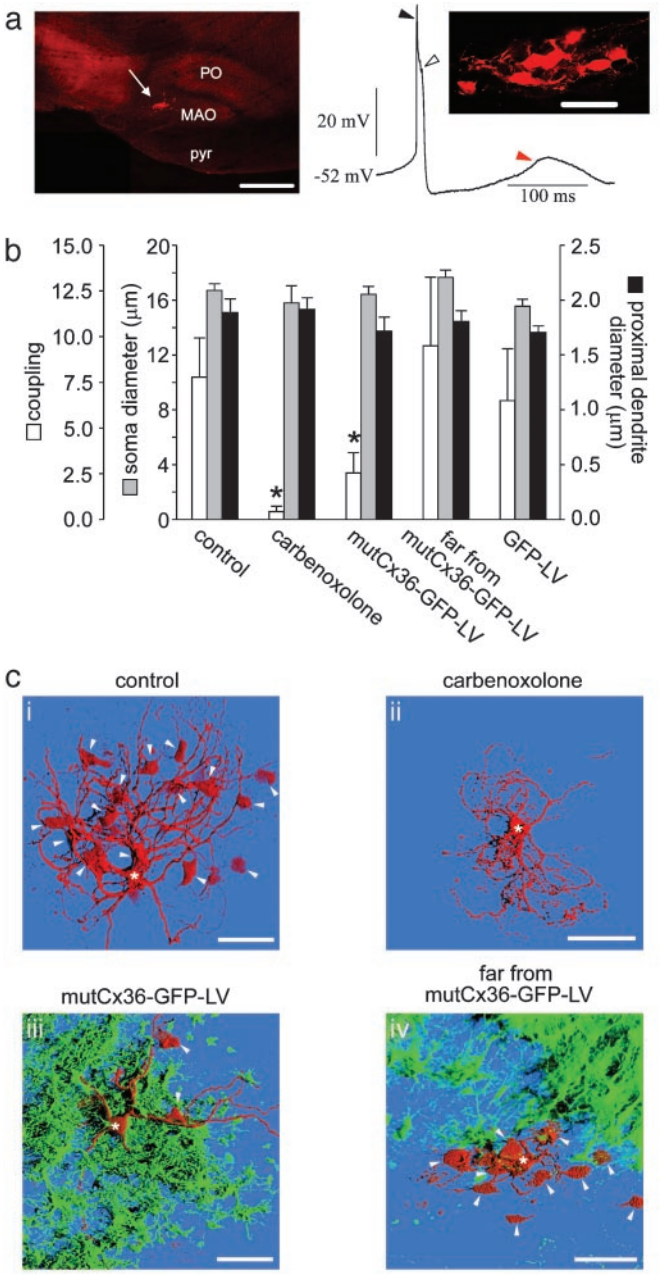

Fig. 3. mutCx36-GFP-LV blocks cytosolic coupling of IO neurons without altering their morphology. (*a*) A sagittal brainstem slice (*Left*) from which an intracellular recording and measurements of cytosolic coupling were obtained (*Right*). Recording confirmed the neuron to be from the IO by the presence of a fast spike (filled arrowhead), after depolarizing potential (open arrowhead), and rebound spike (red arrowhead). PO, principal olive; MAO, medial accessory olive; pyr, pyramid. (*b*) Values of intercellular coupling and neuronal morphology. Coupling was reduced only by carbenoxolone and mutCx36-GFP-LV; there were no morphological differences between the groups. *, $P < 0.05$. (*ci–civ*) Reconstructions of Neurobiotin labeled IO neurons. *, injected somata; arrowheads, coupled neurons; green, GFP. (Scale bars = 500 μm and 50 μm in *a* and 50 μm in *c*.)

min of incubation with 200 μM carbenoxolone ($n = 7$), a pharmacological antagonist of gap junctions (4). Carbenoxolone reduced Neurobiotin spread to 0.4 ± 0.3 neurons ($P < 0.05$; Fig. 3*b*), confirming that the dye spread through gap junctions. In 11 IO neurons recorded from zones transduced by mutCx36-GFP-LV, Neurobiotin spread to 2.5 ± 1.1 neurons (Fig. 3*b*; $P < 0.05$). Cytosolic coupling was normal in 4 IO neurons recorded outside a zone of mutCx36-GFP-LV transduction (9.5 ± 3.8 coupled neurons, $P = 0.71$; Fig. 3*b*), and the control GFP-LV did not reduce coupling (6.5 ± 2.8 neurons, $n = 6$; $P = 0.74$, Fig. 3*b*). Thus, blockade of cytosolic coupling by mutCx36-GFP-LV was due to the mutant Cx36.

Confocal images illustrated the ability of the mutant Cx36 to block cytosolic coupling. In a control experiment (Fig. 3*ci*), 15 neurons were coupled to a recorded IO neuron, and the group was characterized by intertangled dendritic arbors and coupled somata on the periphery of the plexus. Such anatomy was never seen during carbenoxolone where a single labeled cell was the mode (e.g., Fig. 3*cii*). Fig. 3*ciii* shows an IO neuron within a zone of mutant Cx36 transduction. Here, the soma and dendritic arbor of the recorded neuron, and only one coupled neuron, were seen within the GFP. A coupled neuron was immediately outside the zone of GFP (Fig. 3*ciii*, arrowhead). When dye was injected in an IO neuron 50 μm away from a zone of mutant Cx36 (Fig. 3*civ*), a plexus of dendrites was observed, and dye-coupled somata immediately abutted, but did not enter, the GFP-positive area. That the mutant Cx36 prevented cytosolic coupling between IO neurons was consistent with a dominant-negative action and confirmed an important role for Cx36 in the formation of gap junctions in the IO.

Mutant Cx36 LV Does Not Alter Neuron Morphology. To ensure that the blockade of cytosolic coupling by the mutant Cx36 was not due to an alteration in cell morphology, we measured the

Table 1. Electrical properties of IO neurons after LV or carbenoxolone

	Resting membrane potential, mV	Steady-state input resistance, MOhm	Na^+ spike amplitude, mV	High-threshold Ca^{2+} spike amplitude, mV	Low-threshold Ca^{2+} spike slope, mV/ms
Control	−60.3 ± 1.3 (41)	27.9 ± 3.7 (12)	50.2 ± 1.6 (28)	28.8 ± 1.5 (20)	3.7 ± 0.6 (14)
mutCx36-GFP-LV	−59.8 ± 1.5 (15)	54.8 ± 15.6* (8)	46.3 ± 3.1 (10)	30.4 ± 3.0 (9)	3.1 ± 1.2 (5)
Carbenoxolone					
Before	−63.1 ± 2.9	33.5 ± 4.0	55.1 ± 0.8	37.5 ± 2.9	4.6 ± 1.0
During	−64.3 ± 2.3 (11)	43.8 ± 5.7* (4)	52.9 ± 2.3 (5)	36.3 ± 1.6 (3)	4.1 ± 0.7 (4)
GFP-LV	−58.3 ± 2.4 (6)	27.8 ± 11.8 (3)	55.9 ± 5.3 (3)	33.2 ± 4.9 (4)	ND

*, $P < 0.05$ as compared with control. ND, not determined. Numbers in parentheses indicate the number of neurons tested.

thickness of the proximal dendrites and soma of transduced IO neurons (Fig. 3*b*). Control neurons had somata 16.7 ± 0.5 μm wide ($n = 26$) and proximal dendrites 1.9 ± 0.1 μm thick ($n = 34$). Neither parameter was altered by mutCx36-GFP-LV (16.4 ± 0.6 μm, $n = 24$; 1.7 ± 0.1 μm, $n = 19$), GFP-LV (15.5 ± 0.5 μm, $n = 34$; 1.7 ± 0.1 μm, $n = 36$) or carbenoxolone (15.8 ± 1.3 μm, $n = 4$; 1.9 ± 0.1 μm, $n = 20$; all $P > 0.05$). IO neurons located away from zones transduced with mutCx36-GFP-LV were also normal (17.7 ± 0.5 μm, $n = 33$; 1.8 ± 0.1 μm, $n = 20$).

Electrical Properties of IO Neurons Are Unaffected by Mutant Cx36. Table 1 shows the electrical properties of IO neurons from all

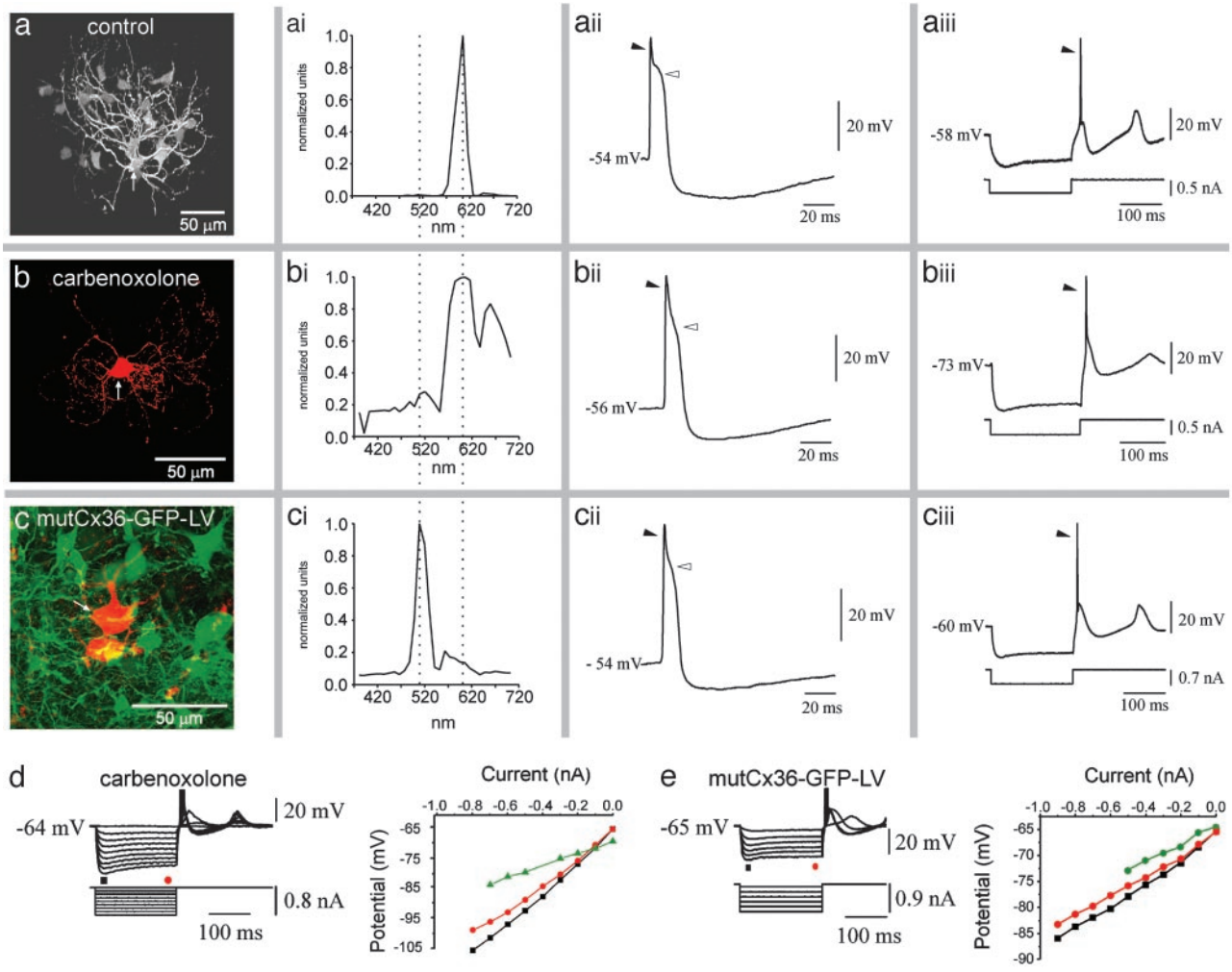

Fig. 4. mutCx36-GFP-LV increases input resistance without affecting electrical properties. (*a–c*) IO neurons recorded and injected with Neurobiotin under control conditions (*a*), during carbenoxolone (*b*), and after transduction with mutCx36-GFP-LV (*c*). Emission of the recorded neurons (arrows) is shown in *ai*, *bi*, and *ci* (488 nm excitation). Only the neuron in *c* shows a peak at 509 nm, indicating GFP. Spikes fired from a depolarized state are shown in *aii*, *bii*, and *cii*; rebound spikes following hyperpolarization are shown in *aiii*, *biii*, and *ciii*. (*d* and *e*) I-V functions recorded from a neuron treated with carbenoxolone (*d*) and in a zone of mutCx36 (*e*). Sodium spikes are truncated. The plots show prerectification (black squares) and steady-state input resistance (red circles). Green curves show steady-state input resistance under control conditions. The control curve in *d* is from the same neuron before carbenoxolone; in *e*, it is from a typical control neuron.

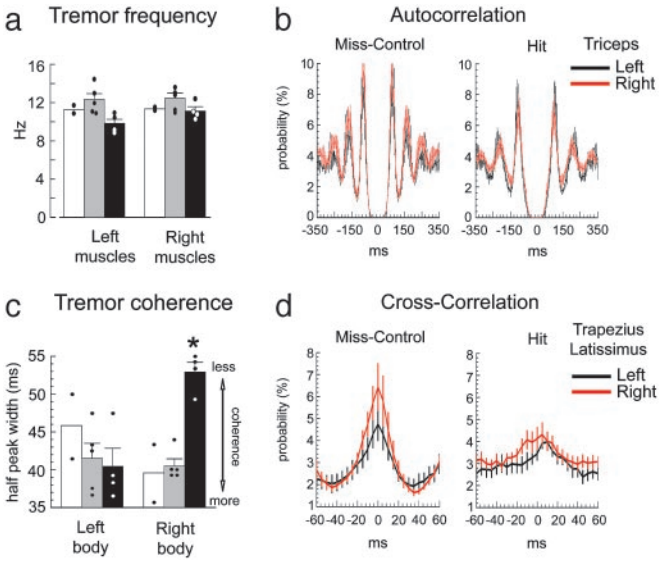

Fig. 5. Blocking Cx36 in the caudal IO impairs the coherence but not rhythm of harmaline tremor. (*a*) Mean tremor frequency for the Hit (black bars), Miss-Control (gray), and GFP-Control (white) groups for left and right side muscles. Dots show single rats. (*b*) Mean auto-correlation functions of tremor from the left and right triceps muscles from the Hit ($n = 4$) and Miss-Control ($n = 5$) groups (111,263 firings). The intervals between peaks were used to compute the tremor frequency of single muscles. (*c*) Mean width of the center peaks of cross-correlograms for the Hit, Miss-Control, and GFP-Control groups for all ipsilateral pairwise comparisons. The value is inversely proportional to coherence and is increased (e.g., coherence reduced) only on the right side of Hit rats, contralateral to the transduction of the IO. *, $P < 0.01$. (*d*) Mean cross-correlation functions of trapezius and latissimus firing relative to ipsilateral triceps. Each curve represents 10 and 8 muscles for the Miss and Hit groups, respectively (248,993 firings). The width of half-amplitude of the center peak was used to compute coherence for each ipsilateral muscle pair.

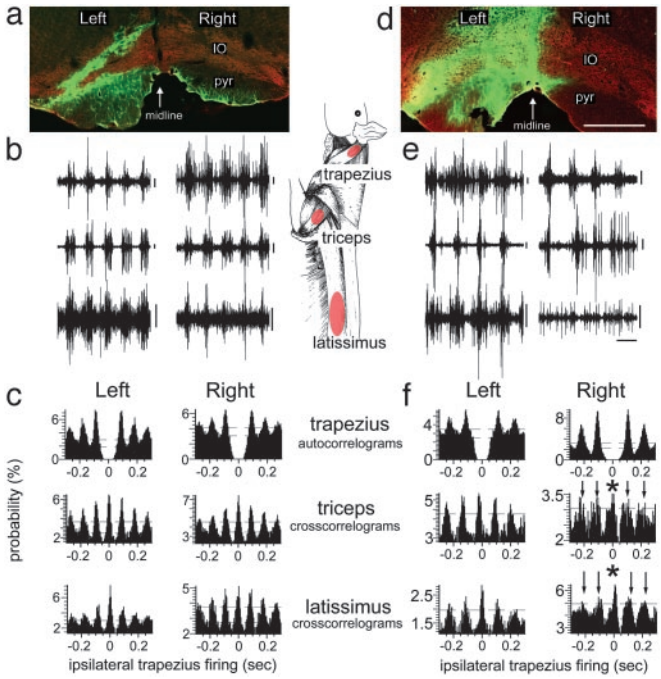

Fig. 6. Harmaline tremor of a Miss (*a*) and Hit (*d*) rat recorded by multisite EMG. In *a* and *d*, red and green show calbindin and GFP, respectively. Correlograms from the Miss and Hit rat are shown in *c* and *f*, respectively, with 500-ms epochs of raw EMG shown above in *b* and *e*. (*Inset*) Muscles recorded. Correlograms are referenced to ipsilateral trapezius. Asterisks and arrows in *f* indicate a broadening of the center and side peaks in the cross-correlograms. Dashed lines indicate 99% confidence intervals. (Scale bars = 0.5 mm in *a* and *d*, and 10 μV and 100 ms in *b* and *e*.)

experimental groups. Under control conditions, spikes triggered from resting potential were comprised of a fast spike, after depolarizing potential, and hyperpolarization (Fig. 4*aii*). When transiently hyperpolarized (Fig. 4*aiii*), a low-threshold spike was triggered at the anode break, which gave rise to a fast spike and often a subsequent low-threshold spike. The fluorescence emission of an example control neuron (488-nm excitation) revealed the presence of the dye (peak at 605 nm) and the absence of GFP (Fig. 4*ai*). The electroresponsiveness of dye-labeled IO neurons during carbenoxolone was the same as the control despite the block of cytosolic coupling (Fig. 4 *bi–biii*).

Fig. 4*c* shows a mutant Cx36-expressing IO neuron, confirmed by GFP emission (Fig. 4*ci*). Although there was only one dye-coupled neuron, the firing of the neuron was unchanged from control (Fig. 4*cii*). In no LV-transduced neuron did we observe the unusual spikes that were present in the hyperpolarized state of IO neurons after embryonic deletion of the Cx36 gene (15) (Fig. 4*ciii*). Moreover, the mutant Cx36 did not change the propensity for spike rhythmicity; second rebound spikes after release from hyperpolarization were seen in three of eight control neurons (8.2 ± 0.5 Hz), in three of six mutant Cx36-transduced neurons (7.8 ± 0.8 Hz), and in two of four neurons during carbenoxolone (6.2 Hz).

Both carbenoxolone and the mutant Cx36 ($n = 8$, $P < 0.05$) increased input resistance when compared with controls, consistent with the reduction of membrane permeability seen in the coupling experiments. Because both morphology and electrical properties were unaffected by the mutant Cx36, we concluded that LV transduction of IO neurons with the dominant-negative Cx36 specifically blocked native Cx36.

Mutant Cx36 in the IO Degrades the Coherence of Harmaline Tremor. We tested the role of Cx36 in harmaline tremor with bilateral, multisite EMG recordings. Because harmaline induces tremor by activating the caudal IO (13, 14) and each IO influences the opposite side of the body through a crossed projection to the cerebellum, we hypothesized that disrupting Cx36 unilaterally in the left IO would alter tremor on the right side of the body exclusively. The design allowed each rat to serve as its own control because the right IO was not transduced and harmaline was given systemically.

Postmortem histology yielded three groups. Four rats received mutCx36-GFP-LV directly in the left caudal IO (Hit group). In 5 rats (Miss-Control), mutCx36-GFP-LV was placed outside the left caudal IO. In these cases, the LV did not transduce caudal IO neurons but transduced the interstices between the subnuclei of the left IO, the rostral IO, the reticular formation, or the raphe. Two rats received GFP-LV that transduced the left caudal IO (GFP-Control).

In an analysis of 42 auto-correlograms from six muscles (Fig. 5*a*), the mean tremor frequency for control rats was 12.0 ± 0.5 Hz and 12.0 ± 0.5 Hz for the left and right side of the body, respectively. The mean tremor frequency derived from 24 auto-correlograms of the Hit rats was 9.8 ± 0.4 Hz and 11.1 ± 0.5 Hz for the left and right side, respectively. There was not a significant lateralization of the tremor rhythm among the groups ($F_{1,7} = 2.7, P > 0.1$). Mean triceps auto-correlograms calculated from all rats in the Miss (KS-Z = 0.95, $P = 0.3$) and Hit (KS-Z = 1.2, $P = 0.09$) groups illustrated the equally rhythmic tremor across the midline (Fig. 5*b*). Thus, unilateral blockade of Cx36 in the caudal IO did not block harmaline tremor or impair its rhythm.

Cross-correlation of the multisite EMG revealed that mutant Cx36 in the left caudal IO reduced the coherence of tremor on

the right side of the body. The reduction in coherence was detected as a significant broadening of the center peaks in the cross-correlograms for comparisons of the right body muscles (52.9 ± 1.4 ms), both as a within-subject contrast to the left (40.3 ± 2.8 ms; $P < 0.001$) and as a between-subject contrast to the Miss-Control rats (41.4 ± 1.1 ms; $P < 0.001$; Fig. 5*c*). ANOVA indicated a significant group by side interaction ($F_{1,7} = 26.4, P < 0.01$). Computed as a difference, the width of the center peak in the right side cross-correlograms of the Hit group was 13 ± 2 ms broader than the left ($P = 0.01$ as different from zero) whereas this value was −1 ± 1 ms for the control, which did not differ from zero ($P = 0.5$). For the Miss-Control group, the mean cross-correlograms of the trapezius and latissimus firing relative to triceps revealed remarkable synchrony among ipsilateral muscles (peak at time 0 in the cross-correlograms in Fig. 5*d*) and did not differ among the body sides (KS-Z = 0.71, $P = 0.7$). For Hit cases, in contrast, the mean of the trapezius and latissimus cross-correlograms relative to triceps were significantly different (KS-Z = 2.1, $P < 0.001$) and showed center peaks that were offset between the sides of the body (Fig. 5*d*).

Fig. 6 shows two cases. In a Miss-Control case (Fig. 6*a*), tremor of the triceps and latissimus on both sides of the body were equivalently synchronous with the ipsilateral trapezius (Fig. 6 *b* and *c*). In a Hit case (Fig. 6 *d* and *e*), tremor was seen in all muscles but was more synchronous on the left as indicated by the sharper peaks in the left side cross-correlograms. The increased variation at time 0 in the cross-correlograms of the right side (Fig. 6*f*, asterisks) resulted in greater dispersion later, apparent in the broader side peaks. The lateralization of the reduction in tremor coherence conformed to the crossed influence of the IO on the body.

Discussion

The findings demonstrate an importance for Cx36 in the olivocerebellar system for movement. Cx36 forms the gap junctions that link the cytosol of neurons and comprises electrical synapses (1–3). *In vivo* neurophysiology has suggested that the synchrony in the output of the IO underlain by electrical coupling is involved in the timing of movement (9). The present results support that view by showing a 10- to 20-ms degradation in the fine temporal coordination of muscle firing after disrupting Cx36 in the IO.

The degradation in the coherence of muscle firing after blocking Cx36 in the IO occurred without a change in the rhythm of harmaline tremor. The absence of an effect on tremor rhythm makes clear that harmaline's tremorogenic action can be mediated by potentiating rhythmic firing at the single neuron level and that collections of uncoupled neurons can become phase locked by circuitry mechanisms. Cx36-mediated coupling tightens the synchrony of IO output and, in turn, allows muscles to be tightly synchronized during a movement, even when many spinal levels separate them.

Previous experiments have shown that global Cx36 "knockout" did not alter gross motricity (11) or prevent harmaline tremor (11, 12). Our results obtained with a very different approach confirm that finding. However, gross tests of movement are insensitive to the function of Cx36 because the advantage that IO Cx36 adds to movement timing is in the range of tens of milliseconds.

Here, we used an approach to knock-down Cx36 function *in vivo*. The use of LV to express a dominant negative Cx36 in the adult IO eliminates the need for embryonic gene deletion, which can generate unpredictable developmental changes (15), and ensures spatial specificity by virtue of having surgical control of where the LV is placed. Although LV-mediated gene transfer has the potential to generate side-effects, our studies have so far indicated no adverse effects of transduction, *per se*, or the expression of the mutant Cx36 on neuron morphology and electrophysiology.

It has been suggested that physiological tremor provides a synchronizing rhythm that confers accuracy to the timing of muscle contractions (26) and that the IO may generate this rhythm (27) to phasically control movement (28). The cocontractions of muscles underlying the most precise movements, such as targeted ball throwing (29), require 10-ms accuracy. Activation of the IO during skilled movement (9) or *in vitro* (30, 31) is manifested as dynamically changing clusters of rhythmically synchronous activity in epochs of 10–30 ms. Our study shows that Cx36 and, by extension, electrical synapses in the IO add 10–20 ms of precision to the temporal coordination of muscle firing during tremor, indicating that electrical synapses in the IO will have their greatest importance for movements requiring millisecond precision among coactive muscles, consistent with the increase in speed that electrical synapses provide over chemical synapses.

We thank M. Mendez, Drs. S. Aicher and M. Dickinson, and Dr. F. Cicirata for Cx36 cDNA. This work was supported by National Institutes of Health Grants NS31224 and RR016858 (to J.P.W.) and DK047754 and DK56465 (to H.-P.K).

1. Condorelli, D. F., Parenti, R., Spinella, F., Trovato Salinaro, A., Belluardo, N., Cardile, V. & Cicirata F. (1998) *Eur. J. Neurosci.* **10,** 1202–1208.
2. Rash, J. E., Staines, W. A., Yasumura, T., Patel, D., Furman, C. S., Stelmack, G. L. & Nagy, J. I. (2000) *Proc. Natl. Acad. Sci. USA* **97,** 7573–7578.
3. Rash, J. E., Yasumura, T., Dudek, F. E. & Nagy, J. I. (2001) *J. Neurosci.* **21,** 1983–2000.
4. Rozental, R., Srinivas, M. & Spray, D. C. (2001) *Methods Mol. Biol.* **154,** 447–476.
5. Llinás, R., Baker, R. & Sotelo, C. (1974) *J. Neurophysiol.* **37,** 560–571.
6. Sotelo, C., Llinás, R. & Baker, R. (1974) *J. Neurophysiol.* **37,** 541–559.
7. Llinás, R. & Yarom, Y. (1981) *J. Physiol. (London)* **315,** 549–567.
8. Llinás, R. & Sasaki, K. (1989) *Eur. J. Neurosci.* **1,** 587–602.
9. Welsh, J. P., Lang, E. J., Sugihara, I. & Llinás, R. (1995) *Nature* **374,** 453–457.
10. Welsh, J. P. (2002) *Ann. N.Y. Acad. Sci.* **978,** 188–204.
11. Kistler, W. M., DeJeu M. T. G., Elgersma, Y., Van der Giessen, R. S., Hensbroek, R., Luo, C., Koekkoek, K. E., Hoogenraad, C. C., Hamers, F. P. T., Gueldenagel, M., *et al.* (2002) *Ann. N.Y. Acad. Sci.* **978,** 391–404.
12. Long, M. A., Deans, M. R., Paul, D. L. & Connors, B. W. (2002) *J. Neurosci.* **22,** 10898–10895.
13. DeMontigny, C. & Lamarre, Y. (1973) *Brain Res.* **53,** 81–95.
14. Llinás, R. & Volkind, R. A. (1973) *Exp. Brain Res.* **18,** 69–87.
15. De Zeeuw, C. I., Chorev, E., Devor, A., Manor, Y., Van Der Giessen, R. S., De Jeu, M. T., Hoogenraad, C. C., Bijman, J., Ruigrok, T. J., *et al.* (2003) *J. Neurosci.* **23,** 4700–4711.
16. Dull, T., Zufferey, R., Kelly, M., Mandel, R. J., Nguyen, M., Trono, D. & Naldini, L. (1998) *J. Virol.* **72,** 8463–8471.
17. Zufferey, R., Dull, T., Mandel, R. J., Bukovsky, A., Quiroz, D., Naldini, L. & Trono, D. (1998) *J. Virol.* **72,** 9873–9880.
18. Naldini, L., Blömer, U., Gallay, P., Ory, D., Mulligan, R., Gage, F. H., Verma, I. M. & Trono, D. (1996) *Science* **272,** 263–267.
19. Placantonakis, D. G., Cicirata, F. & Welsh, J. P. (2002) *Brain Res. Mol. Brain Res.* **98,** 15–28.
20. Zennou, V., Serguera, C., Sarkis, C., Colin, P., Perret, E., Mallet, J. & Charneau, P. (2001) *Nat. Biotechnol.* **19,** 446–450.
21. Placantonakis, D. G., Schwarz, C. & Welsh, J. P. (2000) *J. Physiol. (London)* **524,** 833–851.
22. Placantonakis, D. G. & Welsh, J. P. (2001) *J. Physiol. (London)* **534,** 123–140.
23. Llinás, R. & Yarom, Y. (1981) *J. Physiol. (London)* **315,** 569–584.
24. Devor, A. & Yarom, Y. (2002) *J. Neurophysiol.* **87,** 3048–3058.
25. Winer, B. J. (1971) *Statistical Principles in Experimental Design* (McGraw–Hill, New York).
26. Goodman, D. & Kelso, J. A. S. (1983) *Exp. Brain Res.* **49,** 419–431.
27. Llinás, R. (1991) in *Motor Control: Concepts and Issues*, eds. Humphrey, D. R. & Freund, H. J. (Wiley, London), pp. 223–242.
28. Llinás, R. (1970) in *The Neurosciences: Second Study Program*, ed. Schmitt, F. O. (The Rockefeller Univ. Press, New York), pp. 409–426.
29. Timman, D., Citron, R., Watts, S. & Hore, J. (1999) *J. Neurophysiol.* **86,** 2690–2702.
30. Devor, A. & Yarom, Y. (2002) *J. Neurophysiol.* **87,** 3059–3069.
31. Leznik, E., Makarenko, V. & Llinás, R. (2002) *J. Neurosci.* **22,** 2804–2815.